J|A|C|S ARTICLES

Published on Web 09/08/2009

Probing Surface Accessibility of Proteins Using Paramagnetic Relaxation in Solid-State NMR Spectroscopy

Rasmus Linser,[†] Uwe Fink,[†] and Bernd Reif*[,†,‡]

Leibniz-Forschungsinstitut für Molekulare Pharmakologie (FMP), Robert-Rössle-Str. 10, D-13125 Berlin, Germany and Charité Universitätsmedizin, D-10115 Berlin, Germany

Received May 13, 2009; E-mail: reif@fmp-berlin.de

Abstract: Paramagnetic Relaxation Enhancement (PRE) can be used to accelerate NMR data acquisition by reducing the longitudinal proton relaxation time T_1 in the solid state. We show that the presence of paramagnetic compounds in the bulk solvent induces a site-specific relaxation in addition to local dynamics, which is dependent on the surface accessibility of the respective amide proton in the protein. Differentiation between paramagnetic relaxation and dynamics was achieved by a comparison of ^{1}H T_1 times obtained from microcrystalline protein samples prepared with different concentrations of the Cu^{II}(edta) chelate. We find that relaxation can in addition be mediated by hydroxyl groups, which transfer relaxation by their ability to exchange with the quickly relaxing bulk solvent. Furthermore, relaxation seems to be transferred by water molecules which diffuse into the protein structure and yield an efficient difference PRE in flexible regions of the protein. The experiments are demonstrated using a perdeuterated sample of the α-spectrin SH3 domain, which was microcrystallized from a buffer containing 90% D_2O. Deuteration is a prerequisite to avoid spin diffusion which would otherwise compromise site specific resolution.

Introduction

Accessibility measurements can be used as a tool for the characterization of protein−protein interaction interfaces and for the identification of binding sites in proteins. Protein interaction surfaces have been mapped by H/D exchange.[1,2] In addition to in-silico modeling[3] and chemical modifications in combination with mass spectrometry,[4,5] NMR has been used to obtain information on the properties of protein surfaces. In solution-state NMR, protein−protein as well as protein−ligand interfaces can be mapped using intermolecular NOEs[6,7] or chemical shift perturbations.[8,9] Similarly, radicals or paramagnetic ions can be employed to map solvent-exposed residues or short-lived protein−ligand contact interfaces.[10−17] In solution state, proton−solvent distances have been shown to correlate well with paramagnetic proton R_1 relaxation rates in the case of chelated Gd.[18] Use of nickel complexes strongly reduces R_1, whereas R_2 is mostly unaffected.[19] In the literature, increased transverse and longitudinal relaxation due to paramagnetic compounds is coined paramagnetic relaxation enhancement (PRE). The effect originates either from paramagnetic compounds, which are abundantly available in the sample,[20,21] or from a localized unpaired electron, which is introduced for example by site-directed spin-labeling.[22,23] Because of the significant content of solvent in the microcrystalline lattice (on the order of 50%), proteins are exposed to bulk water similarly as in solution. We and others have shown recently that Cu−chelates can be used to achieve an overall relaxation enhancement leading to faster NMR data acquisition in the solid

[†] Leibniz-Forschungsinstitut für Molekulare Pharmakologie (FMP).
[‡] Charité Universitätsmedizin.

(1) Paterson, Y.; Englander, S. W.; Roder, H. *Science* **1990**, *249*, 755–759.
(2) Mandell, J. G.; Falick, A. M.; Komives, E. A. *Proc. Natl. Acad. Sci. U.S.A.* **1998**, *95*, 14705–14710.
(3) Nimrod, G.; Glaser, F.; Steinberg, D.; Ben-Tal, N.; Pupko, T. *Bioinformatics* **2005**, *21*, i328–37.
(4) Aye, T. T.; Low, T. Y.; Sze, S. K. *Anal. Chem.* **2005**, *77*, 5814–5822.
(5) Suckau, D.; Mak, M.; Przybylski, M. *Proc. Natl. Acad. Sci. U.S.A.* **1992**, *89*, 5630–5634.
(6) Clore, G. M.; Gronenborn, A. M. *J. Magn. Reson.* **1982**, *48*, 402–417.
(7) Blommers, M. J. J.; Stark, W.; Jones, C. E.; Head, D.; Owen, C. E.; Jahnke, W. *J. Am. Chem. Soc.* **1999**, *121*, 1949–1953.
(8) Dehner, A.; Furrer, J.; Richter, K.; Schuster, I.; Buchner, J.; Kessler, H. *Eur. J. Chem. Biol.* **2003**, *4*, 870–7.
(9) Schmiedeskamp, M.; Rajagopal, P.; Klevit, R. E. *Protein Sci.* **1997**, *6*, 1835–1848.
(10) Teng, C. L.; Bryant, R. G. *Biophys. J.* **2004**, *86*, 1713–25.
(11) Ulmer, T. S.; Campbell, I. D.; Boyd, J. *J. Magn. Reson.* **2002**, *157*, 181–189.
(12) Ulmer, T. S.; Campbell, I. d.; Boyd, J. *J. Magn. Reson.* **2003**, *166*, 190–201.
(13) Niccolai, N.; Ciutti, A.; Spiga, O.; Scarselli, M.; Bernini, A.; Bracci, L.; Maro, D. D.; Dalvit, C.; Molinari, H.; Esposito, G.; Temussi, P. A. *J. Biol. Chem.* **2001**, *276*, 42455–42461.
(14) Niccolai, N.; Spadaccini, R.; Scarselli, M.; Bernini, A.; Crescenzi, O.; Spig, O.; Ciutti, A.; Marco, D. D.; Bracci, L.; Dalvit, C.; Temussi, P. A. *Protein Sci.* **2007**, *10*, 1498–1507.
(15) Molinari, H.; Esposito, G.; Pegna, M.; Ragona, L.; Niccolai, N.; Zetta, L. *Biophys. J.* **1997**, *73*, 382–396.
(16) Iwahara, J.; Clore, G. M. *Nature* **2006**, *440*, 1227–1230.
(17) Tang, C.; Iwahara, J.; Clore, G. M. *Nature* **2006**, *444*, 383–386.
(18) Pintacuda, G.; Otting, G. *J. Am. Chem. Soc.* **2002**, *124*, 457–471.
(19) Cai, H.; Seu, C.; Kovacs, Z.; Sherry, A. D.; Chen, Y. *J. Am. Chem. Soc.* **2006**, *128*, 13474–13478.
(20) Respondek, M.; Madl, T.; Göbl, C.; Golser, R.; Zangger, K. *J. Am. Chem. Soc.* **2007**, *129*, 5228–5234.
(21) Wickramasinghe, N. P.; Kotecha, M.; Samoson, A.; Paast, J.; Ishii, Y. *J. Magn. Reson.* **2007**, *184*, 310–316.
(22) Battiste, J. L.; Wagner, G. *Biochemistry* **2000**, *39*, 5355–5365.
(23) Nadaud, P. S.; Helmus, J. J.; Kall, S. L.; Jaroniec, C. P. *J. Am. Chem. Soc.* **2009**, *131*, 8108–8120.

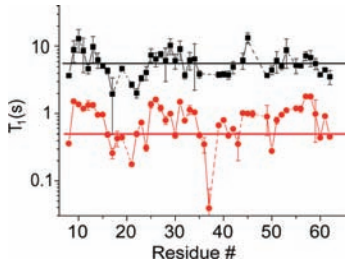

Figure 1. Longitudinal ^{1}H T_1 relaxation times for the SH3 domain of chicken α-spectrin in the absence of Cu^{II}(edta) (black squares) and in the presence of 75 mM Cu^{II}(edta) (red circles). The average T_1 for the amide protons amounts to 5.6 and 0.49 s in the absence and presence of the paramagnetic solute, respectively.

state.[21,24] ^{1}H T_1 relaxation times can be drastically reduced if Cu^{II}(edta) is added to the protein solution prior to crystallization.[21,24,25] Acceleration of the measurement of up to a factor of 8.4 has been accomplished by fast magic-angle spinning (40 kHz) in combination with low-power decoupling (TPPM with ϖ_{RF} = ca. 10 kHz, [Cu^{II}] = 10 mM).[21] Using perdeuterated proteins, the relaxation delay of the bulk magnetization can even be reduced by a factor 15 ([Cu^{II}] = 250 mM). This allows us to record experiments that are otherwise very insensitive.[26]

Figure 1 shows the longitudinal H^N T_1 relaxation times for a sample of the SH3 domain of chicken α-spectrin crystallized in the presence of 75 mM Cu^{II}(edta) in comparison with an untreated sample. In the absence of Cu^{II}(edta), we find large site-specific variations of the ^{1}H T_1 relaxation time. These fluctuations are most likely due to local structural fluctuations because dipolar interactions among protons are largely abolished by almost complete deuteration. Upon addition of the metal chelate, the general appearance for relaxation rates as a function of the primary sequence is maintained, although the average H^N T_1 relaxation time is greatly reduced. A closer inspection of the observed $^1H^N$ T_1 times, however, reveals that the decrease in longitudinal relaxation times is not uniform throughout the protein backbone.

The corresponding ^{1}H relaxation R_1 rates are (2.1 ± 3.6) s^{-1} and $(2.2 \pm 1.2) \times 10^{-1}$ s^{-1} in the presence and absence of Cu^{II}, respectively. An increased standard deviation of the relaxation rate in the case of the doped sample is indicative for a larger dispersion of relaxation rates. As with any relaxation mechanism, paramagnetic relaxation is dependent on the distance between the paramagnetic center and the respective nucleus.[27−29] At the same time, paramagnetic relaxation will not affect internal dynamics or chemical exchange. Consequently, the increased dispersion of relaxation rates hints to a differential distance of the nuclei to the unpaired electron, which in turn suggests different solute accessibilities for different residues. Analysis of protein surface accessibilities by PRE thus also seems possible in the solid state. In Figure 2, different accessibilities of individual H^N protons with respect to the Cu^{II} chelate are schematically represented in the structure of the α-spectrin SH3 domain (PDB code 2NUZ).[30] In A, a cross section through the SH3 crystal structure is depicted together with a Cu^{II} chelate in the bulk-water volume. "a" refers to the distance between the H^N proton and the surface of the protein. The distance "b" reflects the radius of the Cu^{II} chelate (4 Å).[31] This value was used as the Connolly probe radius in the calculation of the accessible volume. "c" refers to the estimated distance (∼2.5 Å) between the solvent and the unpaired electron in the Cu^{II} chelate. Distance values "a" and "c" are taken into account in the quantitative analysis described below. In part B of Figure 2, the respective distance values "a" are depicted as a function of the protein primary sequence. We find a maximum distance of ∼7 Å. In the solid state, water accessibilities have been probed by magnetization transfer from water to the protein.[32−34] However, differentiation between bulk water, side chain exchangeable groups, and tightly bound water molecules is very difficult. We show that solvent exposure of amide protons in proteins can be probed by monitoring site-specific variations of amide proton T_1 relaxation enhancement using paramagnetic chelate complexes. We expect this scheme to be useful in the characterization of the solvent accessibility of membrane channels and pores like for example aquaporins,[35,36] as exposed regions are most important for conductance and selectivity.[37] Similarly, the suggested scheme might contribute to answer the question if the interior of amyloid fibrils are filled with solvent.[38−40]

Materials and Methods

Sample Preparation. A u-[^{2}H,^{13}C,^{15}N] isotopically enriched chicken α-spectrin SH3 sample was used for all experiments described in this manuscript. Low levels of protonation were employed to efficiently reduce spin diffusion. The protein was expressed, purified, and recrystallized as reported previously.[41] Crystallization of the Cu-doped sample was performed as described earlier.[24]

NMR Spectroscopy. All experiments were recorded on a Bruker Avance NMR spectrometer operating at a proton Larmor frequency of 700 MHz. The spectrometer is equipped with a standard 3.2 mm ^{1}H/X/Y broadband triple resonance probe. The channels X and Y were tuned to carbon and nitrogen, respectively. The MAS frequency was set to 24 kHz. The nominal probe temperature was adjusted to 2 °C. The effective sample temperature is higher due to MAS induced heating. We estimate the actual sample temperature to be on the order of 22 °C based on the temperature-sensitive HDO resonance.

(24) Linser, R. J.; Chevelkov, V.; Diehl, A.; Reif, B. *J. Magn. Reson.* **2007**, *189*, 209–216.
(25) Wickramasinghe, N. P.; Shaibat, M. A.; Jones, C. R.; Casabianca, L. B.; Dios, A. C. d.; Harwood, J. S.; Ishii, Y. *J. Chem. Phys.* **2008**, *128*, 052210−052210−15.
(26) Linser, R. J.; Fink, U.; Reif, B. *J. Magn. Reson.* **2008**, *193*, 89–93.
(27) Bertini, I.; Luchinat, C.; Parigi, G. *Solution NMR of Paramagnetic Molecules*; Elsevier: Amsterdam, 2001.
(28) Bertini, I.; Felli, I. C.; Luchinat, C.; Parigi, G.; Pierattelli, R. *ChemBioChem* **2007**, *8*, 1422–1429.
(29) Bertini, I.; Luchinat, C.; Parigi, G.; Pierattelli, R. *ChemBioChem* **2005**, *6*, 1536–1549.
(30) Chevelkov, V.; Faelber, K.; Schrey, A.; Rehbein, K.; Diehl, A.; Reif, B. *J. Am. Chem. Soc.* **2007**, *129*, 10195–10200.
(31) Solans, X.; Font-Altaba, M. *Acta Crystallogr.* **1983**, *C39*, 435–438.
(32) Lesage, A.; Böckmann, A. *J. Am. Chem. Soc.* **2003**, *125*, 13336–13337.
(33) Böckmann, A.; Juy, M.; Bettler, E.; Emsley, L.; Galinier, A.; Penin, F.; Lesage, A. *J. Biomol. NMR* **2005**, *32*, 195–207.
(34) Chevelkov, V.; Faelber, K.; Diehl, A.; Heinemann, U.; Oschkinat, H.; Reif, B. *J. Biomol. NMR* **2005**, *31*, 295–310.
(35) Agre, P.; Preston, G. M.; Smith, B. L.; Jung, J. S.; Raina, S.; Moon, C.; Guggino, W. B.; Nielsen, S. *Am. J. Physiol. Renal. Physiol.* **1993**, *265*, F463–F476.
(36) Walz, T.; Hirai, T.; Murata, K.; Heymann, J. B.; Mitsuoka, K.; Fujiyoshi, Y.; Smith, B. L.; Agre, P.; Engel, A. *Nature* **1997**, *387*, 624–627.
(37) Schäffner, A. R. *Planta* **1998**, *204*, 131–139.
(38) Petros, A. M.; Mueller, L.; Kopple, K. D. *Biochemistry* **1990**, *29*, 10045–10048.
(39) Hetényi, A.; Fülöp, L.; Martinek, T. A.; Wéber, E.; Soós, K.; Penke, B. *ChemBioChem* **2008**, *9*, 748–757.
(40) Zhu, M.; Souillac, P. O.; Ionescu-Zanetti, C.; Carter, S. A.; Fink, A. L. *J. Biol. Chem.* **2002**, *227*, 50914–50922.
(41) Chevelkov, V.; Rehbein, K.; Diel, A.; Reif, B. *Angew. Chem., Int. Ed.* **2006**, *45*, 1–5.

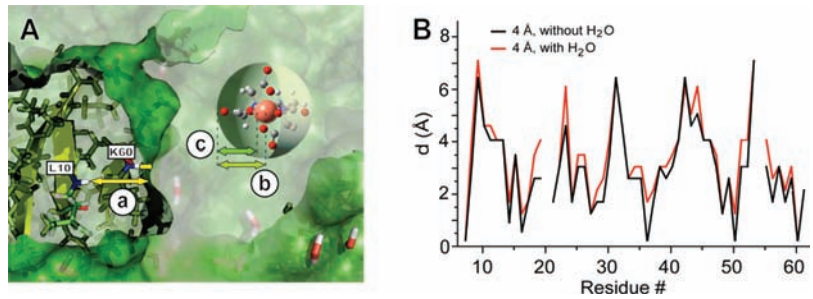

Figure 2. **A**: Cross section of the protein crystal. "a" refers to the distance between the amide proton and the bulk-water accessible volume in the SH3 crystal structure. The interface between the chelate accessible and inaccessible volume was calculated by rolling a spherical probe over the protein lattice performing a Connolly surface calculation. "b" indicates the radius of the probe (4 Å) for the Connolly surface. "c" corresponds to the distance between the chelate surface and the paramagnetic center. **B**: Distances of individual amide protons to the protein surface, obtained by applying the procedure described in **A**. All crystal contacts are taken into account in the calculation. Black and red lines represent the result of the calculation omitting/taking water molecules in the X-ray structure into account, respectively. Residues 20 and 54 are excluded from the calculation (prolines).

T_1 relaxation times were measured using 2D inversion recovery experiments (pulse program shown in Figure 1 of the Supporting Information). In the experiment, ^{1}H magnetization is inverted, followed by a variable delay Δ during which magnetization is allowed to decay. After the 90° ^{1}H read-out pulse, magnetization is transferred to ^{15}N using INEPT for transfer. Nitrogen chemical shift is evolved during t_1, and magnetization is transferred back to protons for detection. Protons and nitrogens are scalar decoupled in the respective evolution periods using 180° composite pulses and WALTZ-16, respectively. Volumes of nonoverlapped cross-peaks were determined using a Gaussian shape fit in both dimensions employing the program *Sparky*.[42] *Origin*[43] was employed to fit the inversion recovery data using a least-squares optimization procedure, assuming a monoexponential decay. Representative decay curves are shown in Figure 2 of the Supporting Information.

Assignment of side chain H^N resonances was obtained via HNCA and HNCACB correlations,[26] yielding C^β and C^α chemical shifts or C^γ and C^β chemical shifts for Asn and Gln side chain resonances, respectively. Down-field shifted H^N resonances were assigned as E (anti to the carbonyl oxygen), upfield shifted proton resonances as Z (syn with respect to the carbonyl oxygen).[44,45]

Distance Calculation. To investigate how the ^{1}H T_1 relaxation time of a specific amide proton is dependent on the proximity to the bulk solvent, quantitative values for the distances between amide protons and the surface of the protein were determined using the X-ray structure of the SH3 domain of α-spectrin at room temperature (PDB entry: 2NUZ) as a reference.[30,34] Protons were included into the structure using *Pymol*.[46] The program *sybyl7.3*[47] was employed to calculate the shortest distances between protons and a potential copper ion: First, the excluded volume that would be inaccessible by the chelated ion due to steric clashes with the protein was defined performing a Connolly[48,49] protein surface calculation using a probe radius reflecting the size of the chelate. As depicted in part A of Figure 2, the chelate was assumed to be a perfect sphere with an approximate radius ("b") of 4 Å.[31] Secondly, all protein atoms were identified that have a certain minimum distance $a_0 <$ 0.5 Å to this protein surface. Subsequently, this minimum distance was increased in steps of $\Delta a = 0.5$ Å to identify more burried amide protons, yielding a dissection of the protein into shells with increasing surface distance. The distances between an individual amide proton and the protein surface vary between 0 Å and 7 Å. For a quantitative data analysis, the geometry of the chelate, in particular, the distance "c" (part A of Figure 2) between the unpaired electron and the surface of the chelate, has to be considered. Connolly surface calculations were performed including/excluding crystallographic water molecules in the structure. The respective distances are drawn in black and red in part B of Figure 2.

Exchangeable side chain protons are treated in a similar fashion. In our case, Gln and Asn side chains turn out to be generally located close to the protein surface. In the crystal lattice, the accessibility for these groups is very high. With the exception of N38, the side chain H^N protons are located directly at the interface to the bulk solvent. N38 is involved in two hydrogen bonds, in particular to T32−OH and I30−CO. Like the backbone amide proton of N38, however, neither of these protons is detectable in solid-state NMR experiments, most likely due to chemical exchange line broadening.

Results

Relaxation. The quantification of paramagnetic relaxation is carried out for a total of 45 residues. Only those residues are analyzed that are clearly resolved in the HSQC spectrum and have sufficient signal-to-noise for a reliable data analysis (below). The corresponding average ^{1}H R_1 relaxation rates amount to (2.1 ± 3.6) s^{-1} and $(2.2 \pm 1.2) \times 10^{-1}$ s^{-1} in the presence and absence of Cu^{II}(edta), respectively (Figure 1). Variations of the ^{1}H R_1 relaxation rates can be due to a certain amount of structural flexibilities in the protein backbone. This is supported by the observed high correlation coefficient between ^{1}H R_1 and ^{15}N R_1 relaxation rates, which suggests that variations in relaxation rates are due to backbone dynamics (data not shown). In general, the overall distribution of R_1 values along the primary sequence is quite similar for both doped and nondoped samples. The larger rmsd in case of the Cu^{II}(edta)-treated sample indicates that additional factors, like for example proximity to the chelate, contribute to the relaxation rate in the presence of Cu^{II}(edta).

Differential PRE. To eliminate contributions from local dynamics, we calculated the ^{1}H difference rate R_1[75 mM Cu^{II}(edta)] − R_1[0 mM Cu^{II}(edta)] as a function of the primary sequence (Figure 3 of the Supporting Information). This difference rate only contains contributions due to paramagnetic relaxation. In addition, relaxation rates were determined from a sample doped with 250 mM Cu−edta to obtain the difference rates R_1[250 mM Cu^{II}(edta)] − R_1[0 mM Cu^{II}(edta)] and R_1[250 mM Cu^{II}(edta)] − R_1[75 mM Cu^{II}(edta)]. The data consistently confirm that the paramagnetic impact on ^{1}H T_1 is a defined site-specific effect. A closer inspection of the difference rates reveals

(42) Goddard, T. D.; Kneller, D. G. *SPARKY 3*; University of California: San Francisco, CA.
(43) *Origin (Version 8)*, OriginLab Corporation: Northampton, MA, 2007.
(44) Löhr, F.; Rüterjans, H. *J. Magn. Reson.* **1997**, *124*, 255–258.
(45) Rajagopal, P.; Jones, B. E.; Klevit, R. E. *J. Biomol. NMR* **1998**, *11*, 205–212.
(46) DeLano, W. L. *The PyMOL Molecular Graphics System DeLano Scientific*; San Carlos, CA, USA, 2002.
(47) *SYBYL 7.3, Tripos International*, 1699 South Hanley Rd., St. Louis, Missouri, 63144, USA.
(48) Connolly, M. L. *J. Appl. Crystallogr.* **1983**, *16*, 548–558.
(49) Connolly, M. L. *Science* **1983**, *221*, 709–713.

that H^N atoms with low PRE are located in regions of the protein, which are far away from the water-accessible surface. This involves in particular those parts of the protein that are implicated in crystal−crystal contacts (e.g., residues 54−59, 25−28, and 10−15). High PRE values are observed for side chain H^N protons. In addition, an increased relaxation enhancement is found in parts of the extended loop including residues E17 to T24.

Paramagnetic spin label tags or solutions containing paramagnetic molecules have been used as probes to measure distances and surface accessibilities in solution-state NMR.[10,11] Transverse relaxation rates R_2 are strongly dependent on the proximity of the paramagnetic center and the respective nuclear spin. This effect is used to obtain long-range distance restraints for structure calculations.[22] Similarly, longitudinal relaxation is induced by the fast electronic transitions of an unpaired electron interacting with a nuclear spin.[27] Generally, the longitudinal relaxation time T_1 is a more sensitive probe to detect paramagnetic centers than the respective transverse relaxation time T_2.[28] Paramagnetic relaxation depends on the distance between the nucleus and the electron. The respective rate is given as[27,28]

$$\Delta R_1 = k/r^6 \tag{1}$$

$$k = \frac{2\gamma_I^2 g_e^2 \mu_B^2}{15} S(S+1)\left(\frac{\mu_0}{4\pi}\right)^2 \times \left[\frac{\tau_c}{1+(\omega_I-\omega_S)^2\tau_c^2} + \frac{3\tau_c}{1+\omega_I^2\tau_c^2} + \frac{6\tau_c}{1+(\omega_I+\omega_S)^2\tau_c^2}\right] \tag{2}$$

with

$$1/\tau_c = 1/\tau_S + 1/\tau_I \tag{3}$$

in which γ_I corresponds to the nuclear gyromagnetic ratio of the nucleus, g_e is the free electron g-factor, S the quantum number associated with the electron spin, r refers to the electron-nucleus distance, and ω_I and ω_S are the Larmor frequencies of the nucleus and electron, respectively. μ_0 and μ_B are related to the vacuum permeability and Bohr's magneton, respectively. τ_c represents the effective correlation time, τ_S the electronic correlation time. While in solution, τ_I refers to the rotational correlation time of the molecule, in the solid state, τ_I represents the correlation time of the local dynamics. Curie relaxation should be largely absent in the solid state, except for a small contribution that is caused by local mobility.[50,51] Longitudinal PRE is only dependent on the distance between the paramagnetic center and the nuclear spin proportional to r^{-6}. All other parameters are invariant in a quantitative analysis of the ^1H difference R_1 rates.

In the case of a soluble paramagnetic chelate, the paramagnetic center S does not adopt a fixed distance r to a given amide proton H^N. Although the relaxation efficiency is highest for chelates approaching the surface of the protein ($r = r_0$), a contribution to ΔR_1 results as well from chelates that are present in the solvent accessible volume. For those remote chelates, a lower relaxation efficiency is partially compensated by the larger number of sites for which the same distance r to the respective amide proton is found.[52,53] The integral contribution to relaxation can be either calculated explicitly using a grid search algorithm taking structural information on the solvent accessible volume into account.[18] Alternatively, the solvent accessible volume surrounding the closest point on the protein surface to any given amide proton H^N can be approximated by analytical integration of the solvent volume associated half-sphere (part A of Figure 4 of the Supporting Information). For a plane protein surface, the distance dependent difference rate ΔR_1 can be written as

$$\Delta R_{1,\mathrm{eff}} = k r_{\mathrm{eff}}^{-6} \tag{4}$$

with

$$r_{\mathrm{eff}}^{-6} = \int_0^{r'_{\max}} \int_0^{2\pi} \int_0^{\pi/2} r^{-6} r'^2 \sin\theta \, \mathrm{d}\theta \, \mathrm{d}\phi \, \mathrm{d}r' \tag{5}$$

and r', φ, θ being the integrands of the spherical integral. r is obtained from

$$r = \sqrt{r_0^2 + r'^2 + 2r_0 r' \cos\theta} \tag{6}$$

In case the surface deviates from planarity, the integration limits for θ are smaller or larger than $\pi/2$, assuming a concave or convex surface, respectively (parts B and C of Figure 4 of the Supporting Information). For small $r'_{\max}$, $r_{\mathrm{eff}}{}^{-6}$ corresponds to $r_0{}^{-6}$. However, for finite sizes of the sphere, the respective function decays considerably more smoothly. Because of the fact that the number of sites at a certain distance to the center is proportional to r'^3, the dipolar interaction is effectively proportional to $r_0{}^{-3}$. This is confirmed numerically. The evaluation of the integral can be approximated well by the function $\Delta R_1 = \mathrm{const} \cdot r_0{}^{-3}$. In the integral, the radial cutoff $r'_{\max}$ was chosen to be 8 Å. This takes into account that the relaxation efficiency quickly decreases for larger distances ($\Delta R_{1,\mathrm{eff}}(r'_{\max}, r_0) = \Delta R_{1,\mathrm{eff}}(r_0)$ for large $r'_{\max}$, Figure 5 of the Supporting Information).

Figure 3 shows the dependence of the longitudinal PRE on the H^N surface distance r_0. The data points fit reasonably well to the expected dependence, which is approximated by a $r_0{}^{-3}$ function. Certain residues, however, deviate from the correlation, in particular E17, S19, E22, T24, I30, T32, and the side chain amide $H^N(Z)$ of Q50. These are excluded in Figure 3 (a complete set of all measured values is shown in Figure 6 of the Supporting Information). We fitted the data employing the function $A(r_0 + B)^{-3} + C$. B reflects the probe specific parameter "c" (part A of Figure 2), which accounts for the distance between the surface of the chelate and the unpaired electron. We find a best fit for $B = 0.5$. Additionally, the fit curve is vertically offset by $C = 0.7\ \mathrm{s}^{-1}$. In addition, simulations assuming a convex and a concave protein surface ($\theta_{\max}$ being 120° and 60°, respectively) are added to the graph.

Discussion

In general, the data confirm the expected r^{-3} proportionality of paramagnetically induced relaxation. The appearance of residues with difference rates larger than theoretically expected (Figure 6 of the Supporting Information) suggests the involvement of parameters other than the surface distance of a H^N proton. To explain these outliers, we consider in the following

(50) Balayssac, S.; Bertini, I.; Lelli, M.; Luchinat, C.; Maletta, M. *J. Am. Chem. Soc.* **2007**, *129*, 2218–2219.
(51) Gueron, M. *J. Magn. Reson.* **1975**, *19*, 58–66.
(52) Ayant, Y.; Belorizky, E.; Fries, P.; Rosset, J. *J. Phys. (Paris)* **1977**, *38*, 325–337.
(53) Vigouroux, C.; Belorizky, E.; Fries, P. H. *Eur. Phys. J. D* **1999**, *5*, 243–255.

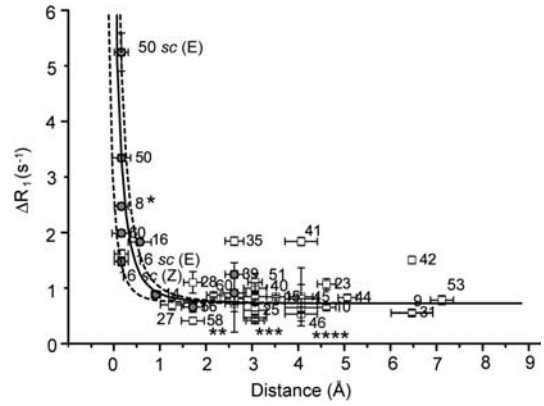

Figure 3. Difference H^N relaxation rate $\Delta R_1 = R_1$[75 mM Cu^{II}(edta)] − R_1[0 mM Cu^{II}(edta)] as a function of the minimum distance r_0 between an individual amide proton and the protein surface. The experimental data are fit assuming a r^{-3} dependence. Amide protons not involved in H-bonds are shown as gray circles. Only H^N protons that are more than 3.5 Å apart from side chain hydroxyl groups are depicted. The surface distance for L8* is calculated assuming a smaller probe radius of 1.4 Å, as L8 is close to a cavity, which is accessible to H_2O but too small for Cu^{II}(edta). Residues 33, 34, 49, 59 (**), 26, 52, 55, 57 (***), and 11, 12, 13 (****) are not labeled due to limitations in space. Labels "E" or "Z" refer to the stereochemistry of the respective side chain ("sc") protons. In addition to simulations using a half-spherical chelate accessible volume, simulations with an underlying concave ($\theta_{max} = 60°$) and convex surface shape ($\theta_{max} = 120°$) are included in the graph (lower and upper dotted lines, respectively).

temporary electrostatic interactions, specific binding of the chelate to the protein and relaxation mediated by chemical exchange or spin diffusion.

Binding and Electrostatic Interaction. As a 4-fold organic acid, edta as well as edta metal ion complexes are negatively charged at physiological pH.[54,55] In solution-state NMR, specific binding of metal chelates to specific regions of the protein has been proposed for Cu^{II}(edta) earlier.[19] This effect, however, could not be observed in the present study, as no amide resonances are significantly attenuated in comparison to the untreated sample, as described before.[26] In addition to the electrostatic attraction to positive partial charges, temporary protein−chelate interactions with side chain hydroxyl- and ammonium-moieties might result in a nonstatistic distribution of residence times of the paramagnetic chelate. Next-neighbor distances between amide protons and side chain nitrogen atoms in the SH3 α-spectrin crystal structure were determined using the *CCP4* software package.[56] This calculation includes all Lys and Arg side chains (Figure 7 of the Supporting Information). We do not find any amide moiety that is in the vicinity ($d < 3.5$ Å) of a NH_3^+ moiety. Positively charged side chains can therefore not serve as an explanation for the unexpectedly high relaxation rates of residues E17, S19, E22, T24, I30, T32, and the Q50 side chain amide H^N(Z). The same is true assuming a proximity of the respective H^N protons to the negatively charged side chains glutamate and aspartate.

Indirect Relaxation Mechanisms. Part A of Figure 4 displays the distance between H^N protons and hydroxyl groups of serine, threonine, and tyrosine. Distance values are represented as d and d^{-6} in the upper and the lower part of the figure, respectively. Residues drawn in light gray denote amino acids in which the respective H^N proton is found to be closer than 3.5 Å to an OH group. In particular, we find that the amide protons of E17, S19, E22, T24, I30, T32, and Q50 side chain amide H^N(Z), as well as K18, R21, S36, T37, and N38 are close in space to a hydroxyl group. For the latter residues, no PRE values are available because the resonances of those residues show low intensities, probably due to exchange broadening. In fact, the proximity of an amide H^N proton to a hydroxyl group is in agreement with the irregular behavior of the respective residues in the PRE−surface accessibility correlation shown in Figure 6 of the Supporting Information. I30−H^N is involved in an intermolecular hydrogen bond to the side chain of T37. The fact that PRE rates are still quite decent for I30 is probably due to the presence of a hydrogen bond between T37−OH and N35−C$\underline{O}$NH_2, which would result in a reduced OH chemical exchange rate for this hydroxyl group (Figure 8 of the Supporting Information).

In the following, the question is addressed if a close proximity of an H^N proton to a side chain hydroxyl group can be the cause for the observed irregularities in the PRE−surface distance correlation. Side chain amine and hydroxyl groups are prone to chemical exchange with bulk solvent protons. Respective rates have been measured by Liepinsh and Otting.[57] Residence times amount to 50 μs for tyrosine and up to 1.5 ms for threonine respectively and can be reduced in the presence of exchange catalysts. Exchange rates for arginine and lysine amines are within the same order of magnitude. Addition of paramagnetic chelates into the crystal lattice does not influence the chemical exchange rates per se. Nevertheless, we find the PRE effect to be significantly stronger for amide protons that are in the vicinity of hydroxyl groups. Similar to the relay NOE effect in solution[58−60] or solid-state NMR,[61,62] we hypothesize that the PRE observed for these H^N protons is mediated by water chemical exchange. Because of their proximity to the metal chelate, bulk-water protons are relaxed significantly faster than protein amide protons. Relaxed bulk-water protons then undergo chemical exchange with side chain hydroxyl protons and efficiently relax nearby H^N protons. In the case of exchange, the PRE difference rate will thus only be dependent on the distance between the amide proton and the side chain exchangeable group. This additional *relay*-PRE seems to apply to amide protons that are within 3−4 Å to a hydroxyl group, which explains the systematically increased PRE difference rates for amide protons in the vicinity of hydroxyl groups.

A small number of amide protons would still not exactly fit the PRE−distance relation. This applies in particular to residues N35, W41, and W42. For these residues, none of the reasons given above applies to explain the larger than expected difference PRE. Figure 5 shows a part of a ^1H,^{15}N scalar correlation spectrum containing the resonances of residues S36 and T37. The depicted spectrum was recorded for a SH3 sample crystallized in the absence of the paramagnetic compound. Clearly, the intensities for S36/T37 are significantly reduced in

(54) Carbonaro, R. F.; Stone, A. T. *Anal. Chem.* **2005**, *77*, 155–164.
(55) Threeprom, J.; Som-Aum, W.; Lin, J.-M. *Anal. Sci.* **2006**, *22*, 1179–1184.
(56) Collaborative Computational Project Number 4. *Acta Crystallogr.* **1994** *D50*, 760−763.
(57) Liepinsh, E.; Otting, G. *Magn. Res. Med.* **2005**, *35*, 30–42.
(58) Otting, G. *Prog. NMR Spectrosc.* **1997**, *31*, 259–285.
(59) Otting, G.; Wüthrich, K. *J. Am. Chem. Soc.* **1989**, *111*, 1871–1875.
(60) Otting, G.; Liepinsh, E.; Wüthrich, K. *J. Am. Chem. Soc.* **1992**, *114*, 7093–7095.
(61) Lesage, A.; Emsley, L.; Penin, F.; Böckmann, A. *J. Am. Chem. Soc.* **2006**, *128*, 8246–8255.
(62) Lesagne, A.; Gardiennet, C.; Loquet, A.; Verel, R.; Pintuacuda, G.; Emley, L.; Meier, B. H.; Böckmann, A. *Angew. Chem., Int. Ed.* **2008**, *47*, 5851–5854.

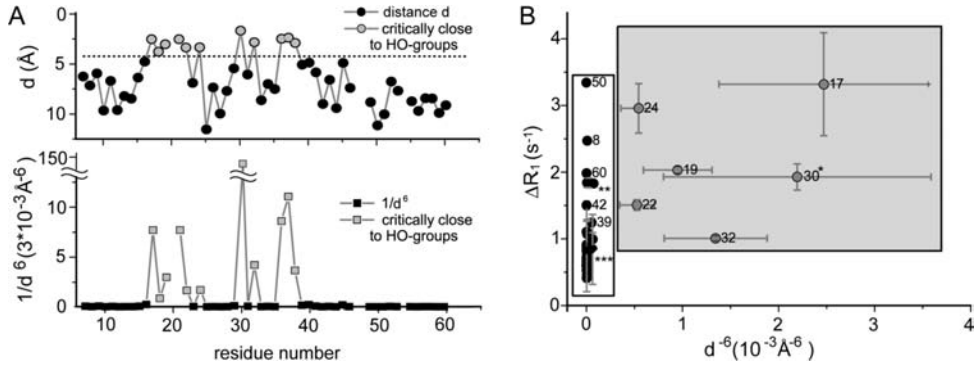

Figure 4. A) Next-neighbor distances d of amide protons to Tyr-, Ser-, or Thr side chain hydroxyl groups. The upper plot depicts the absolute distance, whereas the lower one shows a d^{-6} representation. H^N protons, which are in close proximity to side chain OH groups ($d < 3.5$ Å), are depicted in light gray. B) Correlation between ΔR_1 and d^{-6}. H^N protons close to a OH group show an increased PRE. *: For the plot, d^{-6} for I30 is multiplied by a factor of 1/10. ** and ***: Residue labels of 16, 35, 41 and 9, 10, 11, 12, 13, 14, 15, 23, 25, 26, 27, 28, 31, 33, 34, 40, 44, 45 46, 49, 51, 52, 53, 55, 56, 57, 58, 59, 61, respectively, are not explicitly indicated due to space limitations.

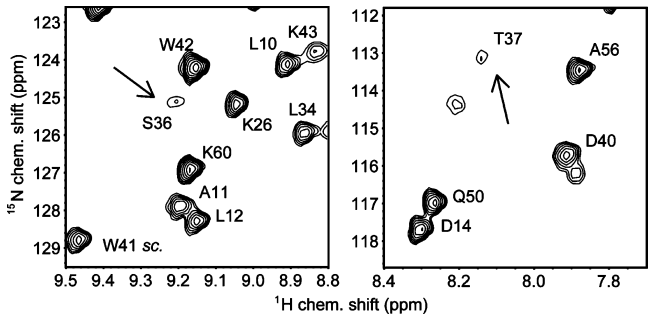

Figure 5. Selected spectral region of a $^1H,^{15}N$ correlation recorded for the SH3 domain of α-spectrin. S36, T37, and N38 show significantly reduced intensities. These amino acids are located in a structurally less defined loop of the protein and are broadened due to chemical exchange. Arrows highlight the resonances of S36 and T37. N38 is not detectable at the employed effective sample temperature (22 °C). The spectrum was recorded using a proton-detected HSQC-type experiment with an indirect ^{15}N chemical shift evolution.

the spectrum, which is indicative for chemical exchange broadening. N38 is not detectable at the employed temperature. Because of their low signal intensities, no PRE values are available for the amide resonances of S36, T37, and N38. Residues 36−39 are located in the n-Src loop between β-sheets $\beta4$ and $\beta5$ in the SH3 structure. A breathing motion of this loop might result in an exchange of water molecules into the structure, yielding an efficient transfer of relaxation also for otherwise inaccessible residues.

The fit curve (Figure 3) correlating the difference PRE and the H^N−surface distance is horizontally shifted by $B = 0.5$ Å, and vertically offset by $C = 0.7\ s^{-1}$. Two reasons can account for the offset B of the abscissa. First, the assumption that Cu−edta is a perfectly spherical particle (8 Å diameter) and that Cu^{II} is situated in the center of the chelate is an oversimplification (Figure 9 of the Supporting Information). Considering a minimal distance between Cu^{II} and the chelate surface of approximately 2.5 Å and a van der Waals radius of Cu^{II} of ∼1.5 Å,[63] the value of $B = 0.5$ Å seems reasonable. Second, water-mediated PRE might induce indirectly amide proton relaxation. In this case, a very small radius "c" (part A of Figure 2) can be assumed for the relaxation inducing agent. The vertical offset of the fit curve ($C = 0.7\ s^{-1}$) has to be interpreted as the result of a non-site-specific transfer of relaxation into the protein. Even though the protein is extensively deuterated, a certain degree of $^1H,^1H$ spin diffusion might lead to relaxation transfer among protons that are dipolar coupled. As a result, a vertical offset of the experimental difference rates would be observed. A more delicate mechanism might involve the transfer of relaxation via freely diffusing water molecules or water protons, assuming that they are able to diffuse into the core of the protein structure.

Conclusion

In this manuscript, we have shown that paramagnetic compounds can provide a measure for the surface accessibility of an amide proton in the solid state. The difference H^N R_1 relaxation rates from samples prepared using different metal chelate concentrations are dependent on the distance between the NMR active nucleus and the unpaired electron of the chelate. We find that relaxation enhancement can be mediated by hydroxyl groups, which transfer relaxation by their ability to exchange rapidly with bulk solvent protons. Furthermore, we observe that flexible regions of the protein exhibit larger than expected PRE difference rates, which is most likely due to water-mediated relaxation. If the specific parameters of the paramagnetic probe are known, information on the proximity of a backbone amide to the hydration water can be deduced from solid-state PRE. For a qualitative analysis, knowledge of the protein structure is not required. Care has to be taken, however, for amide protons that are in close proximity to hydroxyl groups. For those amides, PRE effects are systematically increased, which can result in misinterpretation.

Acknowledgment. We would like to thank Peter Schmieder for continuous support, Katja Faelber for help with in handling the crystal structure and use of the respective programs, and Mangesh Joshi for support with the use of *Sybyl7.3*. This research was supported by the Leibniz-Gemeinschaft and the DFG (Re1435, SFB449, SFB740, FOR475). R.L. is a Kekulé scholar and acknowledges financial support from the Verband der Chemischen Industrie (VCI).

Supporting Information Available: NMR pulse sequence, T_1-relaxation curves, 250 mM Cu-edta-data, integral relaxation effeciency details, complete correlation ΔR_1 vs r_0, distances to positively charged species, molecular environment of I30, atomic model of a chelate molecule. This material is available free of charge via the Internet at http://pubs.acs.org.

JA903892J

(63) Bondi, A. *J. Phys. Chem.* **1964**, *68*, 441–452.